Biochemical and Biophysical Research Communications 373 (2008) 1–7

Contents lists available at ScienceDirect

Biochemical and Biophysical Research Communications

journal homepage: www.elsevier.com/locate/ybbrc

Structure-based inhibitor discovery of *Helicobacter pylori* dehydroquinate synthase

Jai-Shin Liu, Wen-Chi Cheng, Hung-Jung Wang, Yen-Cheng Chen, Wen-Ching Wang *

Institute of Molecular and Cellular Biology and Department of Life Sciences, National Tsing Hua University, 101, Section 2, Kuang-Fu Road, Hsinchu 300, Taiwan

ARTICLE INFO

Article history:
Received 10 May 2008
Available online 27 May 2008

Keywords:
Helicobacter pylori
Shikimate pathway
Dehydroquinate synthase
Docking
Inhibitors

ABSTRACT

Dehydroquinate synthase (DHQS) is a nicotinamide adenine dinucleotide (NAD)-dependent enzyme that converts 3-deoxy-D-arabino-heptulosonate 7-phosphate (DAHP) into 3-dehydroquinate (DHQ). Since it catalyzes the second key step in the shikimate pathway, which is crucial for the aromatic amino acid metabolism in bacteria, fungi, and plants, but not in mammals, DHQS is a potential target for new antimicrobial agents, anti-parasitic agents and herbicides. The crystal structure of *Helicobacter pylori* DHQS (*Hp*DHQS) complexed with NAD has been determined at 2.4-Å resolution and was found to possess an N-terminal Rossmann-fold domain and a C-terminal α-helical domain. Structural comparison reveals that the binary complex adopts an open-state conformation and shares conserved residues in the binding pocket. Virtual docking of compounds into the active site of the *Hp*DHQS structure using the GOLD docking program led to the identification of several inhibitors. The most active compound had an IC_{50} value of 61 μM, which may serve as a lead for potent inhibitors.

Helicobacter pylori is a gram-negative gastric pathogen that colonizes approximately half of the human population and may persist in its presence for a lifetime [1,2]. Enduring infection of this peculiar microbe leads to the chronic inflammation of gastric epithelial cells, which may further progress into peptic ulcers, gastric atrophy, gastric adenocarcinoma and low-grade B-cell lymphoma [2]. *H. pylori* can be eradicated by the standard triple therapy comprised of a proton pump inhibitor and two antibiotic agents [3]. The treatment of *H. pylori* infection using high-dosage antibiotics, however, has resulted in decreased efficacy [4]. Similarly, other resistant organisms including *Staphylococcus aureus* [5] have become more and more difficult to cure. The need for new antibacterial therapies to overcome the problem of antibiotic resistance is therefore a major concern of healthcare professionals.

Current antibiotic agents are targeted towards a relatively small number of proteins (~30), including cross-linking enzymes in the cell wall, ribosomal enzymes, and polymerases in DNA synthesis [6]. One potential approach towards discovering new classes of inhibitors is to target crucial proteins in bacterial but not in mammals. The shikimate pathway which involves seven sequential enzymatic steps in the conversion of erythrose 4-phosphate (E4P) and phosphoenolpyruvate (PEP) into chorismate for subsequent synthesis of aromatic compounds is unique to microbial cells and parasites but absent in animals. Therefore, enzymes of this pathway are attractive targets for the development of non-toxic antimicrobial compounds, herbicides and anti-parasitic agents. Indeed, the sixth-step enzyme, 5-enolpyruvylshikimate 3-phosphate (EPSP) synthase, has been exploited as a target with glyphosate, a well-known herbicide [7].

Dehydroquinate synthase (DHQS) is the second-step enzyme of the shikimate pathway and catalyzes the conversion of 3-deoxy-D-arabino-heptulosonate 7-phosphate (DAHP) into 3-dehydroquinate (DHQ). In an animal model, infection with a knock-out DHQS *Salmonella typhimurium* mutant revealed attenuation in the virulence [8], which supports that DHQS is a potential drug target. The first structure of DHQS from a microbial eukaryote *Aspergillus nidulans* (*An*DHQS) is that of a homodimer [9]. Each subunit consists of an N-terminal Rossmann-fold domain and a C-terminal α-helical domain [9]. The substrate analog carbaphosphonate (CBP), Zn^{2+}, and a cofactor NAD^+ are located in a deep cleft between the N and C domains. Structures of other liganded *An*DHQS complexes (various combinations of NAD, ADP and CBP) suggest a large-scale open-to-closed induced-fit movement of the enzyme upon substrate-binding [10], enabling the catalytic reaction to take place.

Aside from the fungal DHQS structure, the bacterial DHQS structures from *Staphylococcus aureus* (*Sa*DHQS) [11] and *Thermus thermophilus* HB8 (*Tt*DHQS) were recently determined, respectively [12]. Structural comparison between the fungal *An*DHQS and bacterial *Sa*DHQS reveals a homologous architecture but different propagation processes during domain closure, suggesting a structural divergence [11].

In this study, we present the crystal structure of *H. pylori* DHQS (*Hp*DHQS) in complex with NAD. Despite a low sequence identity (30% identity with *An*DHQS, 28% with *Sa*DHQS, 27% with *Tt*DHQS),

* Corresponding author. Fax: +886 3 5717237.
E-mail address: wcwang@life.nthu.edu.tw (W.-C. Wang).

0006-291X/$ - see front matter © 2008 Elsevier Inc. All rights reserved.
doi:10.1016/j.bbrc.2008.05.070

the *Hp*DHQS structure shows a homologous DHQS fold. Structural analysis reveals that the binary complex is present in an open-form conformation and contains conserved substrate-binding residues. Structure-based approach was subsequently employed to identify inhibitors with IC_{50} values in the micromolar range.

Materials and methods

Protein expression and purification. The *aroB* gene encoding *Hp*DHQS was amplified from *H. pylori* 26695 genomic DNA by PCR and inserted into the pQE30 expression vector. The *Hp*DHQS protein was expressed from *E. coli* JM109 cells transformed with pQE30-*Hp*DHQS. The expressed *Hp*DHQS protein was purified by immobilized nickel–ion chromatography.

Preparation of DAHP. 3-Deoxy-D-*arabino*-heptulosonate 7-phosphate (DAHP) was prepared by the enzymatic condensation of D-erythrose 4-phosphate (E4P) and phosphoenolpyruvate (PEP) catalyzed by *Corynebacterium glutamicum* DHAP synthase [13]. The recombinant *C. glutamicum* DHAP synthase was expressed and purified as previously described [13]. The standard reaction mixture (1.0 ml) consisted of 100 μM PEP, 100 μM E4P, 100 μM cobalt chloride in 50 mM Bis–Tris propane buffer (pH 7.4), and 39 nM of the purified *C. glutamicum* DHAP synthase. A spectrophotometric method was utilized to detect the level of the PEP conversion at 232 nm ($\varepsilon = 2800\ M^{-1}\ cm^{-1}$) [14]. The mixture was passed through a column of Dowex 1X8 and DAHP was eluted with 0.6 M HCl as described in [15]. An obvious signal at *m/z* of 287 Da corresponding to that of DAHP was detected [16].

Enzymatic assay. The level of DAHP was determined by a thiobarbiturate assay method [17]. All assays were conducted at 37 °C in a 200-μl solution containing 20 mM Bis–Tris propane buffer (pH 7.0), 0.5 mM DAHP, 0.02 mM cobalt chloride, 0.02 mM NAD^+ and 1 μM *Hp*DHQS. The residual DAHP was oxidized by periodate to produce formylpyruvate, which then reacted with thiobarbiturate to yield a pink adduct, and this chromophore was monitored at A_{549} after extraction into cyclohexanone according to the procedures described in Mehdi et al. [14].

Inhibition assay. Compounds were prepared to 100 mM in dimethylsulfoxide (DMSO) solutions. A 5% DMSO control was included for each set of measurements. About 1 μM *Hp*DHQS was added to the mixture containing the compound to be tested with the standard assay mixture. The test compounds were also evaluated whether they interfered the thiobarbiturate assay system in the absence of *Hp*DHQS. The initial velocities were plotted against the inhibitor concentrations to obtain the IC_{50} by using the following equation

$$A[I] = A[0] \times \{1 - [[I]/([I] + IC_50)]\}$$

where $A[I]$ is the enzyme activity with inhibitor concentration [I], and $A[0]$ is the enzyme activity without the inhibitor.

Crystallization. Crystallization was performed by the hanging-drop vapor-diffusion method at 20 °C using the protein solution (~10 mg/ml) in 50 mM Tris–HCl, pH 8.0. The best crystals were obtained in a solution containing 20 mM NAD, 3.5 M NaFormate, 0.1 M Tris–HCl (pH 7.5). The crystals grew in a cubic form with a maximum size of about 0.3 × 0.3 × 0.3 mm within 7 days.

Data collection and structure determination. The crystals belong to space group *R3* with cell dimensions of *a* = 158.29 Å, *b* = 158.29 Å, and *c* = 97.38 Å, and contain a dimer in the asymmetric unit. Diffraction data were collected at the Macromolecular X-ray Crystallographic Laboratory of National Tsing Hua University, Hsinchu, Taiwan and processed with the HKL suite [18]. All datasets were collected at −150 °C and Fomblin was used as cryoprotectant. Statistics of the collection and the refinement are given in Supplemental Table 1.

The *Hp*DHQS structure was solved by molecular replacement with the program AMoRe [19], using the *An*DHQS · NAD structure (PDB code, 1NRX) as the search template. Rotation and translation functions followed by the rigid body refinement procedure were carried out using data from 8- to 3-Å resolution. Crystallographic refinement was carried out using REFMAC5 program [20] and coupled to ARP/wARP [21]. Omit density maps were produced and inspected after refinement to revise the model manually with the program O [22]. The overall quality of the final model was assessed by the program PROCHECK [23].

Structural comparisons. Structure comparisons with *An*DHQS · NAD (PDB code, 1NRX), *An*DHQS · NAD · CBP (PDB code, 1DQS) [10], *Sa*DHQS · NAD (PDB code, 1XAH), *Sa*DHQS · NAD · CBP (PDB code, 1XAJ) [11] and *Tt*DHQS (PDB code, 1UJN) [12] were carried out using the program LSQMAN in O [22] to superimpose Cα atoms. Combined sequence and secondary structure alignments and figure preparation were done with the program ESPript [24]. Structural figures were prepared with the program PyMOL (www.pymol.org).

Virtual docking. The *Hp*DHQS·NAD·CBP model was prepared using the *An*DHQS·NAD·CBP structure (PDB code, 1DQS) [9] as the template model. The sequence alignment was performed using the ClustalW program [25] and was manually optimized to match

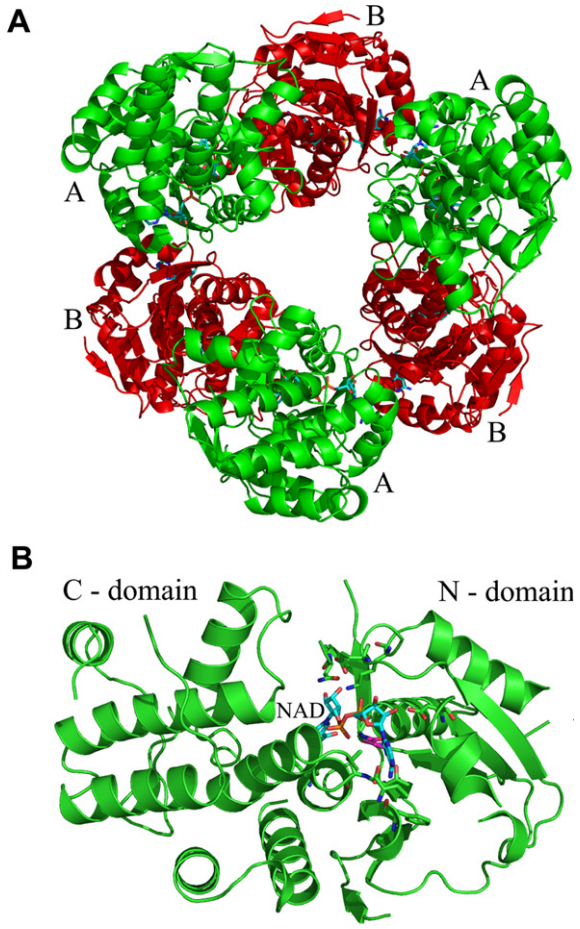

Fig. 1. Structures of *Hp*DHQS. (A) The ribbon representation of hexameric structure $(AB)_3$ viewed down a threefold axis. Three A subunits are depicted in green and the three B subunits are in red. (B) *Hp*DHQS is shown in ribbon model. Each subunit consists of an NAD situated in the cleft between N and C domains. NAD is depicted as sticks with the carbon, oxygen and phosphorus atoms in cyan, red and orange, respectively. G94 and G95 are shown as magenta. (For interpretation of the references to color in this figure legend, the reader is referred to the web version of this paper.)

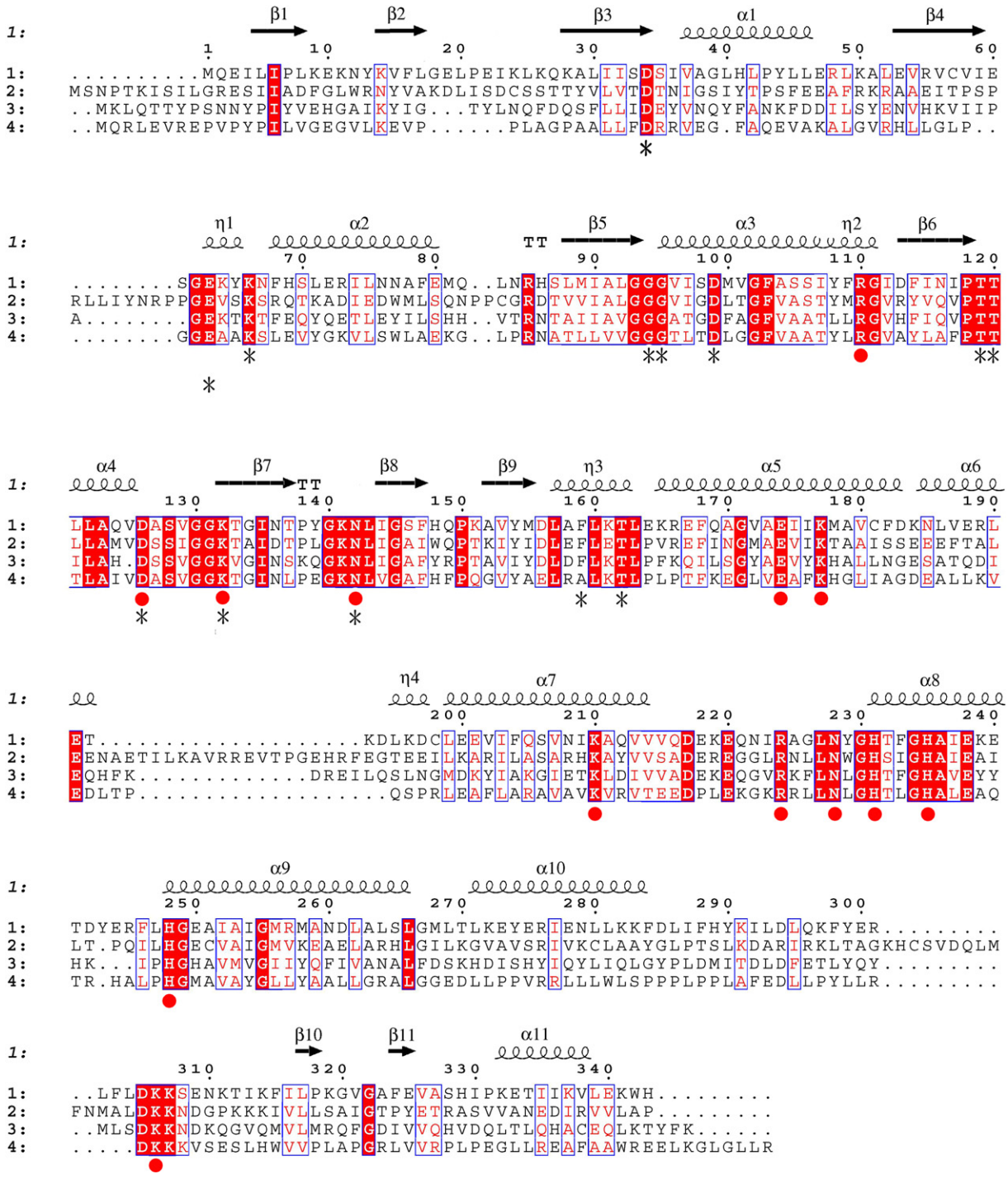

Fig. 2. Structure-based alignments of 3-dehydroquinate synthases. 1, *Helicobacter pylori* 3-dehydroquinate synthase; 2, *Aspegillus nidulans* 3-dehydroquinate synthase; 3, *Staphylococcus aureus* 3-dehydroquinate synthase; 4, *Thermus thermophilus* 3-dehydroquinate synthase; the secondary structural elements are shown above the sequence. NAD-binding residues are indicated as black asterisks. Conserved residues involved in catalysis are indicated as red circles. (For interpretation of the references to color in this figure legend, the reader is referred to the web version of this paper.)

the secondary elements of the conserved N and C domains. Homology module implemented in InsightII software package (Accelrys, San Diego, CA) was used to generate the closed *Hp*DHQS model. MODELLER [26] was then conducted to build 10 full-atoms, in which the best geometry-quality model was selected using PROCHECK [23]. NAD and CBP were sequentially docked into this model using the program GOLD version 2.1 (CCDC Software Limited, Cambridge, U.K.) [27]. The NAD site was defined within a 20-Å radius around the N atom of G95 and the CBP site was within a 10-Å radius around the Nε atom of K132. Standard default parameter settings were used. The three best solutions were obtained until a root mean square (rms) tolerance of 1.5 Å. This ternary complex model was subjected to energy minimization using the CHARMm force field with InsightII package (Version 2005) [28]. This was done by the Steepest Descent minimization and the conjugate gradient minimization until an rms deviation (rmsd) of 0.05. Anolea [29] and Verify3D [28] were used to assess the overall protein quality of the final model.

The Maybridge database that contains 59284 compounds (Tintagel, Cornwall, U.K.) was utilized. The 2D compounds in SDF

format were converted into 3D structures by CONCORD module of Sybyl program (Version 7.1, Tripos Inc., St. Louis, MO). Docking of small molecules into the *Hp*DHQS model was conducted with GOLD version 2.1 [27]. The automatic searching efficiency was set at 200% along with other default parameters to increase the search efficiency. Twenty genetic algorithm (GA) runs were carried out for each compound.

Results and discussion

Structure determination and overall structure description

Despite a number of crystal forms, only one crystal form that was obtained in a solution containing 20 mM NAD diffracted to a high resolution (2.4 Å). The structure was determined by the molecular replacement method using the *An*DHQS · NAD structure as the template. Finally, the model was refined to 2.4-Å resolution with an R and R_{free} of 20.7% and 25.7%, respectively. The overall crystallographic statistics are shown in Supplemental Table 1.

The electron density map of *Hp*DHQS revealed two molecules (AB) per asymmetric unit. Disordered regions that could not be defined include the N-terminal 1–3 segment and two loop regions (215–223 and 292–314). The electron density map showed the presence of a piece of density in each subunit, which could be modeled as a zinc ion in each subunit. Subunits A and B associate into an AB dimer related by a non-crystallographic twofold axis, and three AB dimers assemble into a hexamer along the 3-fold axis (Fig. 1A).

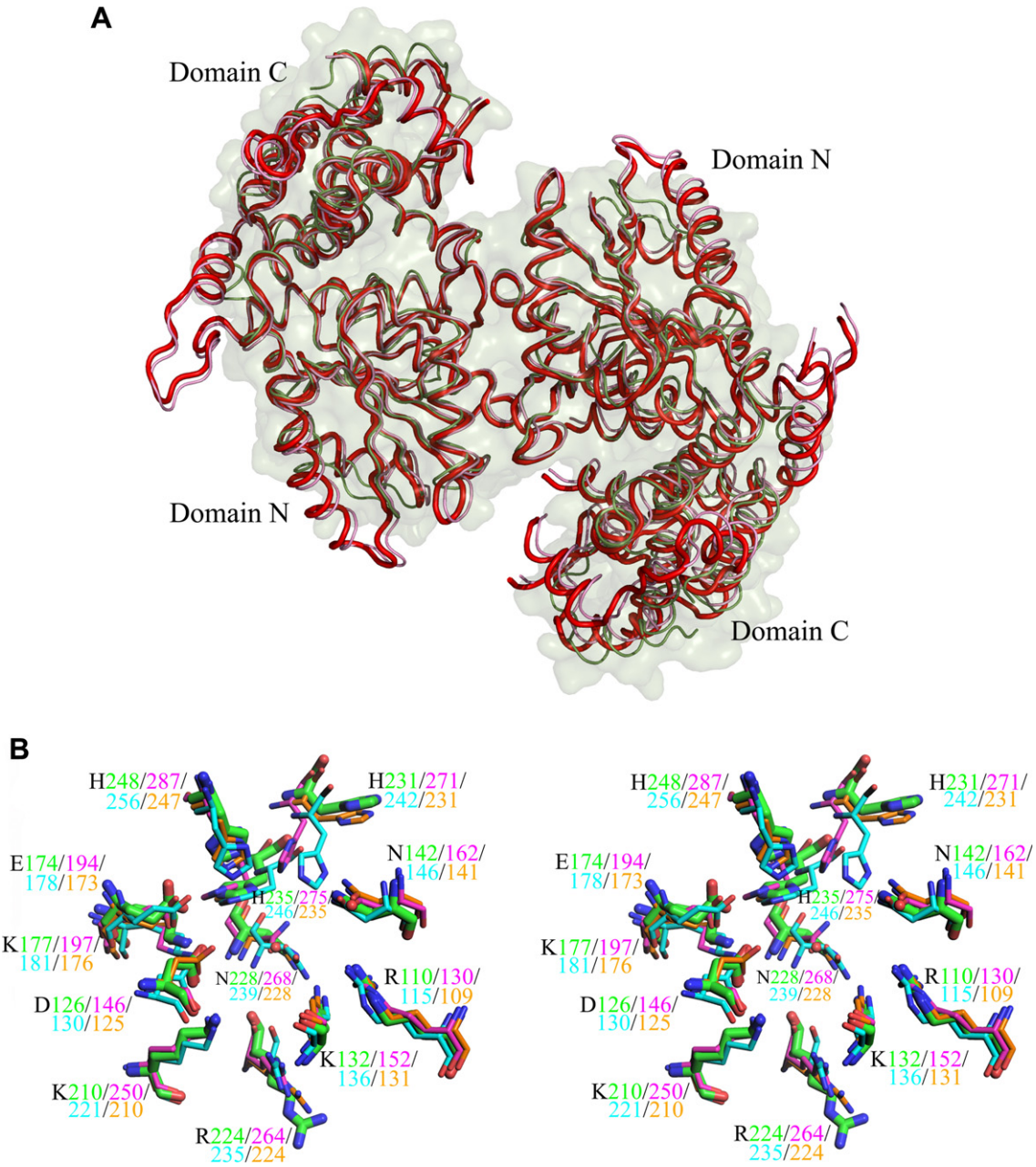

Fig. 3. (A) Superposition of three dimeric DHQSs, *Hp*DHQS·NAD, *An*DHQS·NAD and *An*DHQS·NAD·CBP. *Hp*DHQS·NAD (dark green) and *An*DHQS·NAD (pink) are shown as thin ribbon models and *An*DHQS·NAD·CBP (red) are shown as a thick ribbon model. (B) Stereoview of the active site in the open form DHQSs. Residues in *Hp*DHQS (green) are shown as heavy sticks and those in *An*DHQS (magenta), *Sa*DHQS (cyan) and *Tt*DHQS (orange) are shown as thin sticks. (For interpretation of the references to color in this figure legend, the reader is referred to the web version of this paper.)

Each subunit consists of two domains that are characteristic of other DHQS members (Fig. 1B): (i) the N domain, which has the Rossmann-type architecture, and (ii) the C domain, which contains an α-helical structure. Superimposition of chain A and chain B reveals the essentially overlapping structures (rmsd of Cα atoms = 0.731 Å]. NAD of each subunit is present in the deep cleft, analogous to those observed in other binary structures. The conserved G94 and G95 in the P-loop region make hydrogen-bonding contacts with the phosphate moiety of NAD (Fig. 1B). Other NAD-binding residues include D34, E63, K66, D99, T119, T120, D126, K132, N142, and T162, which are strictly conserved among DHQSs (Fig. 2).

Structural comparison

From on analysis using DALI [30], the *Hp*DHQS structure was found to share structural homology with structures of DHQSs [9–12]. Superimposition with various DHQS structures also reveals modest rmsd values of the overall Cα atoms (1.1−1.6 Å) [9–12].

As has been described in various liganded *An*DHQS and *Sa*DHQS structures, a structural transition from an open to a close state is most likely to take place upon binding to CBP owing to the closure between the N and C domains (differences in domain orientations: AnDHQS, 11–13°; SaDHQS, 8°) [10,11]. We thus compare the domain orientation between the *Hp*DHQS·NAD structure and other DHQS structures. Using the method described in [12], we calculate the rigid-body rotational angle required for the superimposition of the C domains after the primary superimposition at the N domains. Among different DHQSs, the *An*DHQS·NAD complex (open form) showed the least difference (1.8°) in domain orientation as compared with 14.4° for the *An*DHQS·NAD·CBP complex (closed form). These results suggest that the *Hp*DHQS·NAD structure is also present as an open form, as reported for the *Tt*DHQS structure [12].

Analysis of dimeric interactions among various DHQS structures reveals that buried residues involved in the formation of the dimer are from the N domain (α2, α3, η2, β7 and β8). Approximately similar subunit surface areas are used for the formation of the dimer. Notably, a strictly conserved arginine (R110) hydrogen bonds with the peptide O atom (T133) from the neighbor subunit. Based on the optimized alignment of the N domain in the A subunit, superimposition of dimers reveals that the dimeric N domains (corresponding to residues 4–163 in *Hp*DHQS) are well superimposed among *Hp*DHQS·NAD (open), *An*DHQS·NAD (open) and *An*DHQS·NAD·CBP (close) (rmsd in the Cα atoms: *Hp*DHQS·NAD *vs.* *An*DHQS·NAD, 0.66 Å; *Hp*DHQS·NAD *vs.* *An*DHQS·NAD·CBP: 0.67 Å) (Fig. 3A). As expected, there is a large difference in the domain orientation between the open and close forms for each monomer (Fig. 3A). The superimposed C domains exhibit higher deviation in the Cα atom positions (rmsd in the Cα atoms corresponding to residues 164–343 in *Hp*DHQS: *Hp*DHQS·NAD *vs.* *An*DHQS·NAD, 1.20 Å; *Hp*DHQS·NAD *vs.* *An*DHQS·NAD·CBP, 2.05 Å). These results suggest that the N domain contributes to the formation of a closely associated dimer, which may help to maintain the minimal translational mobility of nearby fine-tuned catalytic residues for efficient catalysis [31].

We next compare crucial residues in the binding pockets. As shown in Fig. 2, residues that are responsible for the conversion of DAHP to dehydroquinate in *An*DHQS [9] are conserved among DHQSs. Superimposition of open form DHQS structures shows the virtually identical Cα conformation of these residues in the binding pocket located between the N and C domains (Fig. 3B). Side chains of two residues that correspond to H235 and R224 in *Hp*DHQS are noted as displaying higher deviation. In the presence of CBP, they interact with CBP and are superimposed relatively well between the bound structures (*Sa*DHQS·NAD·CBP and *An*DHQS·NAD·CBP structures). These results together suggest a conserved binding pocket among DHQSs.

Inhibitor screening

Given the conserved binding pocket among DHQSs, we sought to utilize a structure-based approach to search for possible potent inhibitors. The CBP-bound *Hp*DHQS closed model was built using the closed *An*DHQS·NAD·CBP structure as the template model [9]. Superimposition analysis between the *Hp*DHQS·NAD and *Hp*DHQS·NAD·CBP models revealed that either N or C superimposed domains had limited conformational change (rmsd of Cα atoms for the N domains = 0.08 Å; rmsd of Cα atoms for the C domains = 0.65 Å), respectively. The large difference is seen in domain orientation (14.0°), hence supporting that the ternary complex model is a closed form.

Using this model, we then performed virtual screening over the Maybridge database. The docked molecules were ranked by the GOLDScore fitness function and the best 100 molecules were selected. The top ranking compounds that were commercially available were then purchased for inhibitory assay. Seven showed inhibitory action at 500 μM. The two best inhibitors, HTS11955 and RH00573, had IC50 values of 61.0 and 84.4 μM, respectively (Table 1). As compared with the substrate analog CBP that contains a single chair-form ring, both inhibitors consist of two planes that are ~4.5 Å apart. HTS11955 is noted to include has two double-ring planes. Like CBP that contains five functional groups (OH, COOH, and phosphate), these compounds carry N or O atoms and a few functional groups (CN, NH_2, and NO_2) that may hydrogen bond with the nearby residues. Superimposition of these docked models (CBP, HTS11955, and RH00573) shows that these compounds occupy most the CBP site rather than the NAD site (Fig. 4A). One plane from either inhibitor is situated approximately at or near the site of the chair-form ring of CBP. As a result, they make contacts with CBP-interacting residues (⩽3.8 Å), particularly D126, K132, E174, K177, K210, and H231 (Fig. 4B), hence exhibiting their inhibition of DHQS enzymatic activity. These results together suggest a feasible structure-based method for discovering compounds that may be able to be utilized to develop potent inhibitors.

In conclusion, we have determined the 2.4-Å *Hp*DHQS·NAD structure, which is of an open form. The conserved dimeric structural feature seen in all DHQS structures is likely to play a vital role in sustaining the fine-tuned design of active sites. Based on the determined structure, virtual computational screening of a diverse

Table 1
Properties of the DHQS inhibitors

Name	Compound structure	Description
CBP[a]	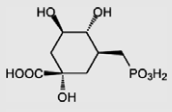	K_i = 0.8 nM
HTS 11955[b]	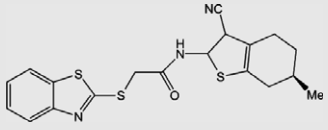	IC_{50} = 61.0 μM
RH 00573[b]	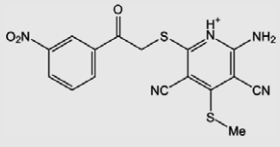	IC_{50} = 84.5 μM

[a] The K_i value of CBP is referred from [32].
[b] This study.

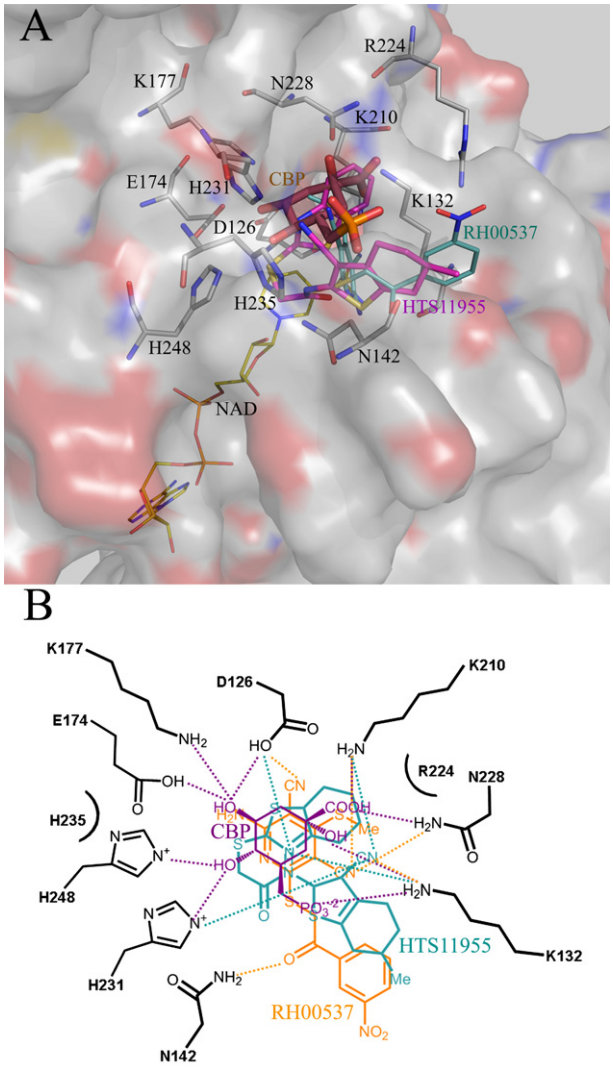

Fig. 4. (A) Molecular surface of *Hp*DHQS with inhibitors. Positive and negative charge areas are blue and red, respectively. NAD is shown as yellow sticks. CBP-interacting residues are shown as thin sticks (grey). CBP (orange), HTS11955 (magenta) and RH00573 (cyan) are indicated as sticks. The oxygen, nitrogen, and sulfur atoms are colored in red, blue and orange, respectively. (B) Schematic representation of interactions between inhibitors and the CBP-interacting residues. The color representation of inhibitors is as in (A). The interactions of hydrogen bond are shown as dash lines. (For interpretation of the references to color in this figure legend, the reader is referred to the web version of this paper.)

set of compounds and inhibition analysis revealed two inhibitors, HTS11955 and RH00573, which may serve as initial leads. Our results demonstrate a feasible structure-based approach to discovering potential inhibitors of DHQS activity.

Protein data bank codes

The atomic coordinates and structural factors for the *Hp*DHQS (code 3CLH) have been deposited in the Protein Data Bank, Research Collaboratory for Structural Bioinformatics, Rutgers University, New Brunswick, NJ (http://www.rcsb.org/).

Acknowledgments

We acknowledge access to the Macromolecular X-ray Crystallographic Center of NTHU Instrument Center at Hsinchu, National Tsing Hua University, Taiwan. We are grateful to the National Center for High-performance Computing for computer time and facilities. This work was supported by the National Science Council (NSC96-3112-B-007-002, NSC96-2313-B-007-001), Taiwan.

Appendix A. Supplementary data

Supplementary data associated with this article can be found, in the online version, at doi:10.1016/j.bbrc.2008.05.070.

References

[1] J.R. Warren, Unidentified curved bacilli on gastric epithelium in active chronic gastritis, Lancet 1 (1983) 1273.
[2] B. Marshall, *Helicobacter pylori*: 20 years on, Clin. Med. 2 (2002) 147–152.
[3] T. Lind, S. Veldhuyzen van Zanten, P. Unge, R. Spiller, E. Bayerdorffer, C. O'Morain, K.D. Bardhan, M. Bradette, N. Chiba, M. Wrangstadh, C. Cederberg, J.P. Idstrom, Eradication of *Helicobacter pylori* using one-week triple therapies combining omeprazole with two antimicrobials: the MACH I Study, Helicobacter 1 (1996) 138–144.
[4] D.Y. Graham, Antibiotic resistance in *Helicobacter pylori*: implications for therapy, Gastroenterology 115 (1998) 1272–1277.
[5] A.F. Shorr, Epidemiology of staphylococcal resistance, Clin. Infect. Dis. 45 (Suppl. 3) (2007) S171–S176.
[6] R. Haselbeck, D. Wall, B. Jiang, T. Ketela, J. Zyskind, H. Bussey, J.G. Foulkes, T. Roemer, Comprehensive essential gene identification as a platform for novel anti-infective drug discovery, Curr. Pharm. Des. 8 (2002) 1155–1172.
[7] H.C. Steinrucken, N. Amrhein, The herbicide glyphosate is a potent inhibitor of 5-enolpyruvyl-shikimic acid-3-phosphate synthase, Biochem. Biophys. Res. Commun. 94 (1980) 1207–1212.
[8] A. Gunel-Ozcan, K.A. Brown, A.G. Allen, D.J. Maskell, Salmonella typhimurium aroB mutants are attentuated in BALB/c mice, Microb. Pathog. 23 (1997) 311–316.
[9] E.P. Carpenter, A.R. Hawkins, J.W. Frost, K.A. Brown, Structure of dehydroquinate synthase reveals an active site capable of multistep catalysis, Nature 394 (1998) 299–302.
[10] C.E. Nichols, J. Ren, H.K. Lamb, A.R. Hawkins, D.K. Stammers, Ligand-induced conformational changes and a mechanism for domain closure in *Aspergillus nidulans* dehydroquinate synthase, J. Mol. Biol. 327 (2003) 129–144.
[11] C.E. Nichols, J. Ren, K. Leslie, B. Dhaliwal, M. Lockyer, I. Charles, A.R. Hawkins, D.K. Stammers, Comparison of ligand-induced conformational changes domain closure mechanisms, between prokaryotic and eukaryotic dehydroquinate synthases, J. Mol. Biol. 343 (2004) 533–546.
[12] M. Sugahara, Y. Nodake, M. Sugahara, N. Kunishima, Crystal structure of dehydroquinate synthase from *Thermus thermophilus* HB8 showing functional importance of the dimeric state, Proteins 58 (2005) 249–252.
[13] C.C. Chen, C.C. Liao, W.H. Hsu, The cloning and nucleotide sequence of a *Corynebacterium glutamicum* 3-deoxy-D-arabinoheptulosonate-7-phosphate synthase gene, FEMS Microbiol. Lett. 107 (1993) 223–229.
[14] S. Mehdi, J.W. Frost, J.R. Knowles, Dehydroquinate synthase from *Escherichia coli*, and its substrate 3-deoxy-D-arabino-heptulosonic acid 7-phosphate, Methods Enzymol. 142 (1987) 306–314.
[15] J.M. Lambert, M.R. Boocock, J.R. Coggins, The 3-dehydroquinate synthase activity of the pentafunctional arom enzyme complex of *Neurospora crassa* is Zn^{2+}-dependent, Biochem. J. 226 (1985) 817–829.
[16] M. Noble, Y. Sinha, A. Kolupaev, O. Demin, D. Earnshaw, F. Tobin, J. West, J.D. Martin, C. Qiu, W.S. Liu, W.E. DeWolf Jr., D. Tew, I.I. Goryanin, The kinetic model of the shikimate pathway as a tool to optimize enzyme assays for high-throughput screening, Biotechnol. Bioeng. 95 (2006) 560–573.
[17] P.R. Srinivasan, D.B. Sprinson, 2-Keto-3-deoxy-D-arabo-heptonic acid 7-phosphate synthetase, J. Biol. Chem. 234 (1959) 716–722.
[18] Z. Otwinowski, W. Minor, Processing of X-ray diffraction data collected in oscillation mode, Methods Enzymol. 276 (1997) 307–326.
[19] J. Navaza, AMoRE: an automated package for molecular replacement, Acta Crystallogr. A 50 (1994) 157–163.
[20] G.N. Murshudov, A.A. Vagin, E.J. Dodson, Refinement of macromolecular structures by the maximum-likelihood method, Acta Crystallogr. D53 (1997) 240–255.
[21] V. Lamzin, K.S. Wilson, Automated refinement of protein models, Acta Crystallogr. D49 (1993) 127–147.
[22] T.A. Jones, J.Y. Zou, S.W. Cowan, M. Kjeldgaard, Improved methods for building protein models in electron density maps and the location of errors in these models, Acta Crystallogr. A 47 (1991) 110–119.
[23] R.A. Laskowski, M.W. MacArthur, D.S. Moss, J.M. Thornton, PROCHECK: a program to check the stereochemical quality of protein structures, J. Appl. Crystallogr. 26 (1993) 283–291.
[24] P. Gouet, E. Courcelle, D.I. Stuart, F. Metoz, ESPript: analysis of multiple sequence alignments in PostScript, Bioinformatics 15 (1999) 305–308.
[25] J.D. Thompson, D.G. Higgins, T.J. Gibson, CLUSTAL W: improving the sensitivity of progressive multiple sequence alignment through sequence weighting, position-specific gap penalties and weight matrix choice, Nucleic Acids Res. 22 (1994) 4673–4680.
[26] A. Sali, T.L. Blundell, Comparative protein modelling by satisfaction of spatial restraints, J. Mol. Biol. 234 (1993) 779–815.

[27] A. Raghuraman, P.D. Mosier, U.R. Desai, Finding a needle in a haystack: development of a combinatorial virtual screening approach for identifying high specificity heparin/heparan sulfate sequence(s), J. Med. Chem. 49 (2006) 3553–3562.
[28] R. Luthy, J.U. Bowie, D. Eisenberg, Assessment of protein models with three-dimensional profiles, Nature 356 (1992) 83–85.
[29] F. Melo, D. Devos, E. Depiereux, E. Feytmans, ANOLEA: a www server to assess protein structures, Proc. Int. Conf. Intell. Syst. Mol. Biol. 5 (1997) 187–190.
[30] I. Bahar, A.R. Atilgan, B. Erman, Direct evaluation of thermal fluctuations in proteins using a single-parameter harmonic potential, Fold Des. 2 (1997) 173–181.
[31] W.C. Chiu, J.Y. You, J.S. Liu, S.K. Hsu, W.H. Hsu, C.H. Shih, J.K. Hwang, W.C. Wang, Structure–stability–activity relationship in covalently cross-linked *N*-carbamoyl D-amino acid amidohydrolase and *N*-acylamino acid racemase, J. Mol. Biol. 359 (2006) 741–753.
[32] J.-L. Montchamp, J.W. Frost, Cyclohexenyl and cyclohexylidene inhibitors of 3-dehydroquinate synthase: active site interactions relevant to enzyme mechanism and inhibitor design, J. Am. Chem. Soc. 119 (1997) 7645–7653.